



Double White Dwarf Merger Products among High-mass White Dwarfs

Sihao Cheng (程思浩)¹, Jeffrey D. Cummings¹, Brice Ménard^{1,2}, and Silvia Toonen³¹ Department of Physics and Astronomy, The Johns Hopkins University, 3400 N Charles Street, Baltimore, MD 21218, USA; s.cheng@jhu.edu² Kavli Institute for the Physics and Mathematics of the Universe, University of Tokyo, Kashiwa 277-8583, Japan³ Institute for Gravitational Wave Astronomy, School of Physics and Astronomy, University of Birmingham, Birmingham B15 2TT, UK

Received 2019 November 12; revised 2020 February 2; accepted 2020 February 4; published 2020 March 16

Abstract

Double white dwarf (double-WD) binaries may merge within a Hubble time and produce high-mass WDs. Compared to other high-mass WDs, the double-WD merger products have higher velocity dispersion because they are older. With the power of *Gaia* data, we show strong evidence for double-WD merger products among high-mass WDs by analyzing the transverse-velocity distribution of more than 1000 high-mass WDs ($0.8\text{--}1.3 M_{\odot}$). We estimate that the fraction of double-WD merger products in our sample is about 20%. We also obtain a precise double-WD merger rate and its mass dependence. Our merger rate estimates are close to binary population synthesis results and support the idea that double-WD mergers may contribute to a significant fraction of type Ia supernovae.

Unified Astronomy Thesaurus concepts: White dwarf stars (1799); Stellar kinematics (1608); Stellar ages (1581); Type Ia supernovae (1728); Bayesian statistics (1900)

1. Introduction

During the last few decades, there has been increasing evidence showing that a large number of double white dwarf (double-WD) systems should merge within a Hubble time (e.g., Marsh 1995, Marsh et al. 1995, Iben et al. 1996, Han 1998, Badenes & Maoz 2012; Maoz et al. 2018; Brown et al. 2020). Many double-WD mergers are believed to produce new white dwarfs (WDs) with higher masses (e.g., Lorén-Aguilar et al. 2009). So, a fraction of high-mass WDs in the solar neighborhood are expected to be double-WD merger products (e.g., Toonen et al. 2017; Temmink et al. 2019). To verify the existence of these merger products, some investigators have looked for an excess of high-mass WDs (Giammichele et al. 2012; Rebassa-Mansergas et al. 2015; Tremblay et al. 2016), and others have searched for kinematic signatures of these merger products (Wegg & Phinney 2012; Dunlap & Clemens 2015). The kinematic method makes use of the following facts: high-mass double-WD merger products are in general older than singly evolved WDs because of their binary evolution, and according to the age–velocity–dispersion relation (AVR) of the Milky Way disk (e.g., Nordström et al. 2004), these older double-WD merger products have higher velocity dispersion. The former method, based on number counts, is influenced by large systematic errors from the adopted initial–final-mass relation of WDs and the sample completeness. In contrast, the kinematic method is less influenced by systematic errors, but it was limited by the sample size of WDs with kinematic measurements.

Thanks to the European Space Agency *Gaia* mission (Gaia Collaboration et al. 2016), the number of stars with precise kinematic measurements has been enlarged drastically. Cheng et al. (2019) selected a deep, homogeneous sample of WDs in a narrow mass range ($1.08\text{--}1.23 M_{\odot}$) from *Gaia* Data Release 2 (DR2; Gaia Collaboration et al. 2018a) to investigate the “Q branch,” an overdensity of WDs on the Hertzsprung–Russell (H-R) diagram, which is caused by a cooling anomaly. As a byproduct of their kinematic analysis, the fraction of double-WD merger products among WDs in their mass range were inferred to be about 22%, and they reserved the task of

conducting an analysis optimized for detecting double-WD merger products and the discussion on this topic to this paper.

In this paper, we extend the kinematic analysis of high-mass WDs to a wider mass range and adopt a more realistic delay-time distribution for binary evolution. We estimate the fractions of double-WD merger products as a function of mass and calculate the corresponding merger rates. We then compare our results to predictions from binary population synthesis. We also discuss the implication of our results for the progenitor problem of type Ia supernovae (SNe), as the double-WD merger is a promising scenario of an SN Ia explosion (e.g., Iben & Tutukov 1984; Webbink 1984).

2. Data

Gaia DR2 provides accurate astrometric (Lindgren et al. 2018) and photometric (Evans et al. 2018; Riello et al. 2018) measurements for more than one billion stars. To search for the kinematic signature of double-WD merger products efficiently, we select nearby, high-mass, hot WDs with precise astrometric and photometric measurements from the *Gaia* DR2 WD catalog compiled by Gentile Fusillo et al. (2019). Below, we introduce in detail our sample selection and the derivation of WD parameters.

We first impose the same quality cuts as Equations (1)–(5) in Cheng et al. (2019) and a distance cut

$$1/\varpi < 250 \text{ pc} \quad (1)$$

to select WDs with high-precision astrometric and photometric measurements. These cuts do not introduce any explicit kinematic biases to our WD sample.

Then, as the kinematic signature of double-WD merger products most outstanding among high-mass, hot (young-photometric-age) WDs, we carry out selections on the photometric mass (m_{WD}) and age (τ_{phot}) of WDs. These cuts, equivalent to cuts on the H-R diagram, are designed to both maximize the sample size and minimize contamination from the standard-mass helium-atmosphere WDs (the “B branch”;

Gaia Collaboration et al. 2018b):

$$\begin{aligned}
 &0.8 M_{\odot} < m_{\text{WD}} < 0.9 M_{\odot}, \\
 &0.1 \text{ Gyr} < \tau_{\text{phot}} < 0.7 \text{ Gyr}; \\
 &\text{or} \\
 &0.9 M_{\odot} < m_{\text{WD}} < 1.28 M_{\odot}, \\
 &0.1 \text{ Gyr} < \tau_{\text{phot}} < 1.0 \text{ Gyr}.
 \end{aligned} \quad (2)$$

The WD parameters m_{WD} and τ_{phot} are derived in the following way. First, we define the absolute-magnitude M_G as $M_G = G + 5 \log(\varpi/\text{mas}^{-1}) - 10$, where G and ϖ are the G -band magnitude and parallax. Then, we convert the H-R diagram coordinate into m_{WD} and cooling time t_{cool} by interpolating a grid of cooling tracks for C/O-core DA (hydrogen atmosphere) WDs (Fontaine et al. 2001) and synthetic colors (Holberg & Bergeron 2006; Kowalski & Saumon 2006; Tremblay et al. 2011).^{4,5} For WDs heavier than $1.07 M_{\odot}$ we use cooling tracks of O/Ne WDs (Camisassa et al. 2019). Finally, the photometric age τ_{phot} is obtained by adding the cooling time t_{cool} to the main-sequence age, which we calculate based on an initial-final mass relation (Cummings et al. 2018) and the relation between precooling time and main-sequence mass from Choi et al. (2016) for nonrotating, solar-metallicity stars.

As shown by Cheng et al. (2019), the “Q branch” on the H-R diagram is produced by an anomalous cooling behavior; some WDs stop cooling and stay on the branch for several billion years, which creates both an overdensity and a high-velocity excess. To avoid modeling the influence of this cooling delay on the velocity distribution and only focus on the binary-evolution delay for double-WD mergers, we exclude the “Q branch” region on the H-R diagram with the following cut

$$M_G < 12.7. \quad (3)$$

We also apply a color cut at the blue end to control the uncertainty of photometric mass and age determination

$$G_{\text{BP}} - G_{\text{RP}} > -0.6. \quad (4)$$

The selection region on the H-R diagram and 1395 selected WDs⁶ are shown in Figure 1.

We divide our selected sample into five mass bins, based on the aforementioned photometric mass (assuming C/O-core below $1.07 M_{\odot}$ and O/Ne-core above it). The edges of bins are 0.8, 0.9, 1.0, 1.1, 1.2, and $1.28 M_{\odot}$. If some WDs heavier than $1.07 M_{\odot}$ are believed to still hold C/O cores instead of O/Ne cores, such as massive double-WD merger products (e.g., Dan et al. 2014), then for those WDs the mass bins correspond to 0.8, 0.9, 1.0, 1.14, 1.24, and $1.32 M_{\odot}$. The sample sizes in these mass bins are 408, 431, 323, 176, and 57, respectively. Because of the absolute-magnitude cut and blue color limit, the photometric-age ranges for the five samples are different. We estimate them to be 0.42, 0.82, 0.86, 0.66, and 0.42 Gyr, respectively.

We estimate the completeness of our sample with the completeness-magnitude relation, $c(G)$, derived in Sollima (2019) by randomly selecting 180 regions in the sky and

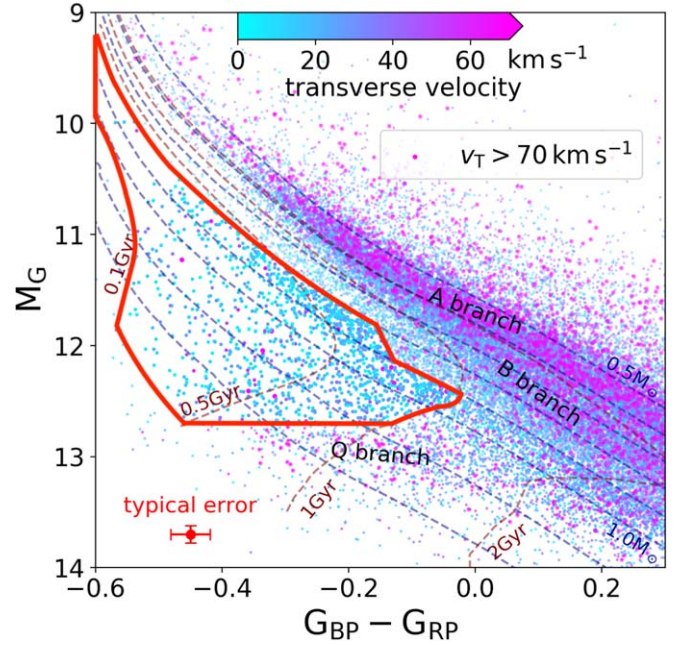


Figure 1. H-R diagram of WDs in *Gaia* DR2. We show a 250 pc sample of WDs with high-quality measurements and a grid of WD masses m_{WD} and photometric ages τ_{phot} derived from the combined O/Ne-core and C/O-core WD cooling model. WDs evolve along their cooling tracks, i.e., the constant-mass curves. The red region includes 1395 nearby, high-mass, hot WDs selected in Section 2 for our kinematic analysis.

comparing *Gaia* DR2 and PanSTARRS DR2 catalogs. His estimate is similar to that given by comparing *Gaia* DR2 and *Hubble Space Telescope* images around globular clusters (Arenou et al. 2018). So, we adopt the relation in Figure 1 of Sollima (2019) and calculate for each mass bin the average completeness, $1/c^{-1}(G_i)$, where G_i represents the G -band magnitude of a single star. The resulting completeness is 88%, 80%, 79%, 79%, and 80%, respectively. In addition, we find that our quality cuts only exclude less than 5% of the objects, given the distance and H-R diagram cuts in Equations (1)–(4).

Finally, we derive the kinematics of WDs, which are related to the true ages of WDs through the AVR. Because *Gaia* does not provide radial velocity information for WDs due to the narrow wavelength coverage of its spectrometer (Gaia Collaboration et al. 2016), we focus on the two components of transverse velocity $v_T = (v_l, v_b)$:

$$v_l = \frac{\mu_l - (A \cos 2l + B) \cos b}{\varpi}, \quad (5)$$

$$v_b = \frac{\mu_b + A \sin 2l \sin b \cos b}{\varpi}, \quad (6)$$

where μ_l and μ_b are the proper motion in the Galactic longitude and latitude directions, and A and B are the Oort constants taken from Bovy (2017).

3. Model

Our goal is to measure the amount of double-WD merger products among high-mass WDs using the kinematic information. According to the AVR, a group of stars with older true stellar age (τ) has higher velocity dispersion. On the other hand, one can derive the photometric isochrone age (τ_{phot}) of WDs from the H-R diagram. If a WD evolves in isolation, τ_{phot} should be equal to τ , whereas if it originates from a double-WD

⁴ <http://www.astro.umontreal.ca/~bergeron/CoolingModels/>

⁵ We made a python 3 package for this kind of transformation, which is publicly available at https://github.com/SihaoCheng/WD_models.

⁶ A catalog of all selected WDs is available on VizieR and at <https://sihaoscheng.github.io/DWDmerger>.

merger event, then an age discrepancy,

$$\Delta t \equiv \tau - \tau_{\text{phot}}, \quad (7)$$

will be created from binary evolution. In general, a WD produced from binary evolution may have positive or negative Δt , but for double-WD mergers with high total mass, the discrepancy is almost always positive (Temmink et al. 2019). So, for a given τ_{phot} , double-WD merger products are older and have higher velocity dispersion.

Following Wegg & Phinney (2012) and Cheng et al. (2019), we assume that the double-WD merger “resets” the WD back to a sufficiently high temperature, so that the real cooling time is equal to the photometric cooling time. Then, Δt can also be expressed as the difference of pre-cooling times between the two evolutionary scenarios, $\Delta t = (\tau - t_{\text{cool}}) - (\tau_{\text{phot}} - t_{\text{cool}})$, where t_{cool} is the cooling time, and the first item $\tau - t_{\text{cool}}$ is sometimes called the “delay time” of double-WD merger. It has been widely used that the distribution of the age discrepancy, $p(\Delta t)$, for double-WD mergers with high total masses is approximately a power law, i.e., $p(\Delta t) \approx \Delta t^{-1}$ (Maoz et al. 2010), because the binary delay time $\tau - t_{\text{cool}}$ is dominated by the double-WD phase when the orbit shrinks due to gravitational-wave emission, and the single-star pre-cooling time $\tau_{\text{phot}} - t_{\text{cool}}$ is negligible. However, in our mass ranges, none of the two statements are valid. So, we use more realistic distributions for Δt , with the binary delay-time distribution, $p(\tau - t_{\text{cool}})$, obtained from binary population synthesis (see Appendix for details) and the values of $\tau_{\text{phot}} - t_{\text{cool}}$ from Section 2.

We consider our WD sample as a mixture of two populations: singly evolved WDs and double-WD merger products,⁷ with fractions $1 - f_m$ and f_m , respectively. If f_m is higher, the tail of the velocity distribution will also be higher, because the double-WD merger products are on average older. For the velocity distribution, we assume that stars with the same true age τ have a Gaussian velocity distribution $\mathbf{v} \sim \mathcal{N}(\mathbf{v}_0(\tau), \Sigma(\tau))$ relative to the Sun (e.g., Binney & Tremaine 2008). The size of this Gaussian distribution is determined by τ through the AVR, and the center of this Gaussian distribution is determined by the solar motion and the age-dependent asymmetric drift $(\sigma_U(\tau)^2/80 \text{ km s}^{-1})$.

We use the same Bayesian framework as constructed by Cheng et al. (2019) to infer the fraction f_m from the photometric age τ_{phot} and transverse velocity \mathbf{v}_T of each WD. This model uses the conditional probability of \mathbf{v}_T given τ_{phot} and other observables as the likelihood function, and thus it eliminates spatial selection biases. In the model, we set f_m and the solar motion as free parameters and adopt the best-fitting AVR in Cheng et al. (2019), a flat star-formation history in our sample volume, and the delay-time distribution of double-WD mergers shown in the Appendix. We do not need to model the “extra cooling delay” included in Cheng et al. (2019) because this delay has no effect in our selected region. We do not include WD kick effects in our model, because for single-evolved WDs, the kick velocity during the WD formation is less than 1 km s^{-1} (El-Badry & Rix 2018), and for double-WD mergers, the kick velocity during merger is a few km s^{-1} (e.g., Dan et al. 2014), which have only a tiny contribution to the increase of velocity

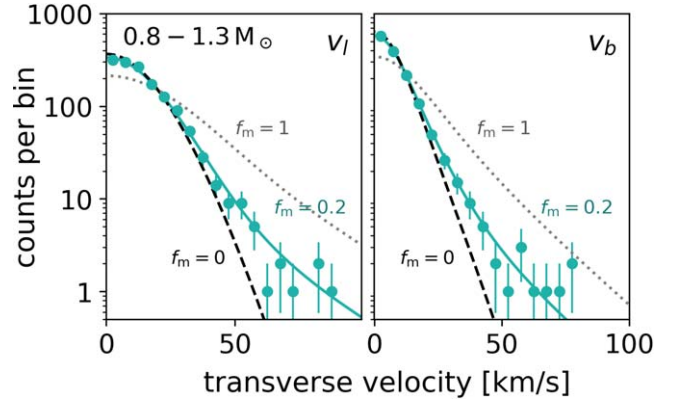


Figure 2. Velocity distribution of our WD sample. We show the sample of WDs from all five mass bins ($0.8\text{--}1.3 M_{\odot}$) as an example. v_l and v_b in the left and right panel of the figure means the Galactic longitude and latitude components of the transverse velocity. We present the observed histograms of the absolute values of v_l and v_b in 20 bins between 0 and 100 km s^{-1} and Poisson errors. We also show the theoretical velocity distributions for $f_m = 0$, 1 , and the average of best-fitting values weighted by the sample size in each mass bin, which is about 0.2 . Note that the y-axes are in logarithmic scale.

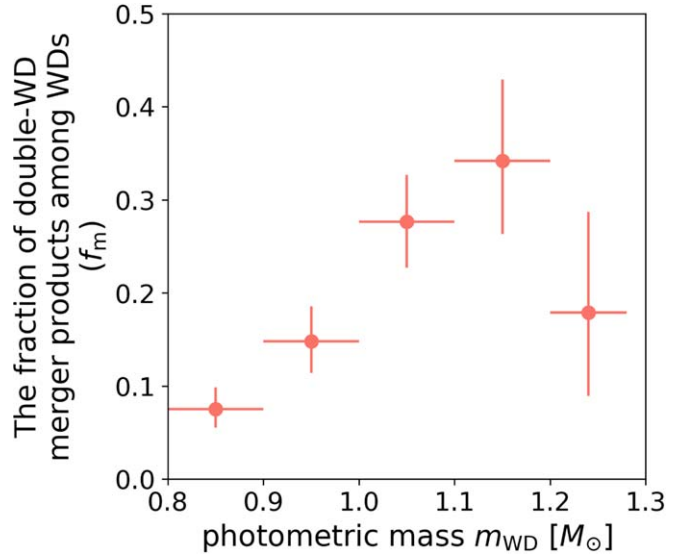


Figure 3. Our estimates for the fraction of double-WD merger products among high-mass WDs, in five bins of WD photometric mass. The sample sizes in these mass bins, from lower to higher masses, are 408, 431, 323, 176, and 57, respectively.

dispersion compared to the contribution from the binary-evolution delay.

4. Results and Discussions

4.1. Constraints on the Fraction of Merger Products

With a sample of high-mass WDs selected from *Gaia* DR2 30 times as large, we are allowed to go beyond Wegg & Phinney (2012) and set strong constraints on f_m . Figure 2 illustrates the transverse-velocity distribution of WDs in our sample. The clear velocity excess is strong evidence for the existence of double-WD merger products. For clarity we only show the distribution of the whole sample, i.e., the combination of all five mass bins, but similar results can be found in each single mass bin, too. In Figure 3, we show our estimate of f_m in each mass bin. We find that the fraction of double-WD mergers

⁷ The high-mass WDs originating from other types of mergers such as main-sequence and giant star mergers have much shorter age discrepancy Δt than that of double-WD mergers. So, in terms of kinematics, we treat the merger products of other types the same as singly evolved WDs.

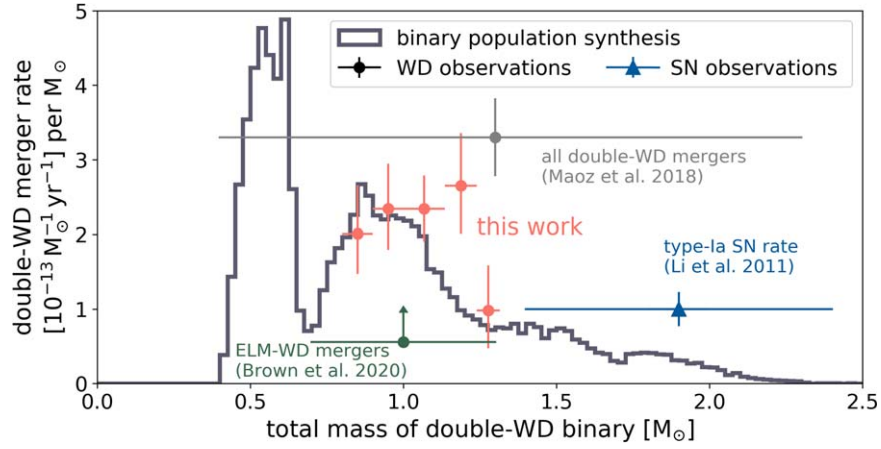


Figure 4. A comparison of the observed and simulated double-WD merger rate. The red data points with error bars are our observational estimates based on double-WD merger products. The histogram shows binary population synthesis results. Other data points show estimates in the literature based on the orbital distribution of observed double-WD systems: the light-gray one is an estimate for all double-WD mergers (Maoz et al. 2018), and the green one is for systems with at least one extremely low-mass (ELM) WD (Brown et al. 2020), which provides a lower limit of the merger rate. The blue data point shows the observed SN Ia rate. Comparisons between a data point and the histogram should be made in terms of the area under the horizontal “error bar” of the data point and the area under the histogram in the same mass range.

Table 1
Measurements of the Double-WD (DWD) Merger Rate and SNe Ia Rate

Reference	Event Rate ($10^{-13} M_{\odot}^{-1} \text{yr}^{-1}$)	Event Type	Based on
This work	0.20 ± 0.06	DWD mergers that produce $0.8\text{--}0.9 M_{\odot}$ WDs	Merger products among single WDs
	0.23 ± 0.06	DWD mergers that produce $0.9\text{--}1.0 M_{\odot}$ WDs	
	0.32 ± 0.06	DWD mergers that produce $1.0\text{--}1.14 M_{\odot}$ WDs	
	0.28 ± 0.07	DWD mergers that produce $1.14\text{--}1.24 M_{\odot}$ WDs	
	0.07 ± 0.04	DWD mergers that produce $1.24\text{--}1.32 M_{\odot}$ WDs	
This work (summed)	1.1 ± 0.3	DWD mergers that produce $0.8\text{--}1.32 M_{\odot}$ WDs	Merger products among single WDs
Maoz et al. (2018)	6.3 ± 1.0	All DWD mergers	Orbital distribution of DWD systems
Brown et al. (2020)	0.3 ± 0.2	DWD mergers with at least one ELM WD	Orbital distribution of DWD systems
Li et al. (2011)	1.0 ± 0.3	SNe Ia in a Milky Way-like galaxy	Extragalactic SNe

in our mass range of $0.8\text{--}1.3 M_{\odot}$ varies from 10% to 35%, with an average of about 20%. This fraction is roughly constant as a function of mass, though declines at the two end are suggested.

To test the robustness of our results, we check for the influence of sample selection, the adopted star-formation history, and the adopted AVR in our model. We found that a different distance cut such as 200 or 300 pc cuts and a linearly decreasing star-formation history with a five times higher rate at 11 Gyr ago have less than 20% fractional influence on the estimate of f_m . For the influence of the AVR, our results are mostly influenced by the 0–4 Gyr part, where the delay-time distribution is peaked. Adopting the high-velocity dispersion from Just & Jahreiß (2010) as used by Wegg & Phinney (2012) will reduce f_m by a factor of 2, but given the observational constraints from both main-sequence stars (e.g., Nordström et al. 2004) and WDs (Cheng et al. 2019), such high values of velocity dispersion are unlikely. The effect of adopted delay-time distribution can be seen from the comparison between our results in the mass range of $1.08\text{--}1.23 M_{\odot}$ and that of Cheng et al. (2019): adopting a power-law delay-time distribution leads to a result about 30% lower. So, we estimate the fractional systematic error of our results as 30% (a factor of 0.7–1.3). Our estimate of f_m is consistent with population synthesis results (Temmink et al. 2019).

4.2. Double-WD Merger Rate

The fraction of double-WD merger products (f_m) obtained in Section 4.1 can be translated into double-WD merger rates. Because our sample is nearly volume limited, the merger rate in each mass bin can be estimated by

$$\text{merger rate} = \frac{f_m \cdot N}{m_{\star} \cdot \Delta\tau_{\text{phot}} \cdot c}, \quad (8)$$

where N is the sample size of each mass bin (listed in the caption of Figure 3), m_{\star} the stellar mass of the Milky Way within 250 pc. $\Delta\tau_{\text{phot}}$ and c are the photometric-age range and sample completeness of each mass bin, which are estimated in Section 2. The stellar mass m_{\star} is estimated to be $4.1 \times 10^6 M_{\odot}$, using the local stellar mass density $\rho_{\star} = 0.083 M_{\odot} \text{pc}^{-3}$ (McMillan 2011) and a scale-height 300 pc of the disk. We list our estimate of the current double-WD merger rate in each mass bin in Table 1. The total merger rate in our mass range ($0.8\text{--}1.3 M_{\odot}$) amounts to $1.1 \times 10^{-13} M_{\odot}^{-1} \text{yr}^{-1}$. To make comparison with other measurements easier, we also divide these values by their corresponding mass ranges and show the results in Figure 4. Note that the mass range of each bin here is slightly different from that in Figure 3, because we

adopt the photometric masses derived from CO WD models (see Section 2 and Table 1 for details).

There are several factors that may lead us to underestimating the merger rate within our mass range. For example, we take the mass of the merger products as the total mass of the original double-WD binary. This is true for CO–CO WD mergers (e.g., Dan et al. 2014) but not for He–CO WD mergers, which may lose significant amount of mass during the R Coronae Borealis phase and produce WDs with $0.6\text{--}0.7 M_{\odot}$ (Schwab 2019). So, we are likely to underestimate the merger rate of systems with original mass below $1.0 M_{\odot}$, where He–CO WD mergers become important. Similarly, we will miss explosive and disruptive merger events if there are any such events in our mass range, and events that result in extremely magnetic and faint WDs (Bhattacharya et al. 2018) if there are such objects produced.

In Figure 4, we also show the merger rate from binary population synthesis, with a flat star-formation history assumed. If a decreasing star-formation rate was assumed, as the delay-time distribution is low for mergers with a long delay time, the synthesis would predict a lower current merger rate than plotted in Figure 4. Details of the population synthesis are shown in the Appendix. We find that the synthesized merger rates are close to our observational estimates without any tuning of parameters. Note that in our analysis of *Gaia* WDs, we only use the distribution of the delay time but never use the total merger rate information from the population synthesis. So, the match between the observed and synthesized merger rate is not a circular argument but rather a validation of our understanding of binary evolution.

Then, we compare our results with other estimates of the double-WD merger rate in the literature. While we count the products of mergers, other estimates are obtained by observing premerger systems and predicting the merger rate. Maoz et al. (2012, 2018), Badenes & Maoz (2012), and Maoz & Hallakoun (2017) extrapolate the orbital distribution of double-WD binaries to estimate the total double-WD merger rate, with an up-to-date estimate being $(6.3 \pm 1.0) \times 10^{-13} M_{\odot}^{-1} \text{ yr}^{-1}$. Brown et al. (2016b; 2020) estimate the merger rate of double-WD binaries with at least one ELM ($< 0.3 M_{\odot}$) WD to be $2 \times 10^{-3} \text{ yr}^{-1}$ in the Milky Way, corresponding to $0.3 \times 10^{-13} M_{\odot}^{-1} \text{ yr}^{-1}$, with a 110% uncertainty including a 70% statistical uncertainty. In Table 1 we list these values. In Figure 4 we assign reasonable mass ranges to these measurements and present the results. For the result from Maoz et al. (2018), we assign $0.4\text{--}2.3 M_{\odot}$ according to the mass distribution in our binary population synthesis, and for the result from Brown et al. (2020), we assign $0.7\text{--}1.3 M_{\odot}$ according to the mass distribution of ELM binaries (Brown et al. 2016a). All data points on Figure 4 should be understood as the averaged merger rate within the assigned mass range. As these measurements address the merger rates of systems in different mass ranges, one cannot compare them directly. But, if we are allowed to use the mass distribution from binary population synthesis to scale these estimates, we will find that the merger rate obtained by Maoz et al. (2018) is about two to three times our estimates, and the estimate from Brown et al. (2020) is consistent with our results, as illustrated in Figure 4. As discussed in Maoz et al. (2018), if the merger rates are as high as their estimate, almost all high-mass WDs will need to be double-WD merger products, which is hard to believe given

the velocity distribution we observe. Nevertheless, it is noticeable that the observational constraints of the double-WD merger rate from different methods have converged to within a factor of a few.

In summary, our estimates of the double-WD merger rate add significant precision and mass resolution to our knowledge of the double-WD merger rate and provide a validation for current binary population synthesis.

4.3. Implication for SNe Ia

SNe Ia are important distance indicators, element factories, interstellar medium heaters, and cosmic-ray accelerators, but their progenitors remain unclear (e.g., Maoz et al. 2014). The double-WD merger is a promising scenario of SN Ia (e.g., Iben & Tutukov 1984; Webbink 1984; Tutukov et al. 1992; Maoz et al. 2010; Mennekens et al. 2010; Sato et al. 2015; Liu et al. 2017; Shen et al. 2018a, 2018b; Perets et al. 2019). The comparison between double-WD merger rate and the SN Ia rate is a critical test from this scenario. When a flat star-formation history is assumed, our population synthesis (Appendix) provides a merger rate of about $0.3 \times 10^{-13} M_{\odot}^{-1} \text{ yr}^{-1}$ for super-Chandrasekhar double-WD systems, which is about 1/7 of the total synthesized double-WD merger rate and consistent with previous studies (e.g., Ruiter et al. 2009; Yungelson & Kuranov 2017). For the D^6 (dynamically driven double-degenerate double-detonation) scenario (e.g., Shen et al. 2018b), a lower rate is obtained, because it requires in general higher total mass of the system (see Figure 2 of Shen et al. 2017).

On the other hand, the observed SN Ia rate for a Milky Way-like galaxy (Sb-Sbc type) is $(1.0 \pm 0.3) \times 10^{-13} M_{\odot}^{-1} \text{ yr}^{-1}$ (Li et al. 2011), or $1.3 \times 10^{-3} M_{\odot}^{-1}$ in terms of a time-integrated rate (Maoz & Graur 2017). This is close to, though two to three times higher than, the synthesized rate for the super-Chandrasekhar and D^6 double-WD merger scenario. As discussed in Section 4.2, our estimates of the double-WD merger rate within $0.8\text{--}1.3 M_{\odot}$ are in agreement with population synthesis results. So, if we are allowed to extrapolate the merger rate to high masses according to the mass distribution of mergers from simulations, then

1. our measurements support the idea that double-WD mergers contribute a significant fraction to SNe Ia;
2. if all SNe Ia come from double-WD mergers, it seems that there exist other explosion mechanisms whose requirement on the total mass of the binary is lower than that of the Chandrasekhar and D^6 explosion models.

5. Conclusion

The merger of two WDs in a close binary system may result in a new WD with higher mass. Therefore, among the high-mass WDs observed today, a fraction should come from double-WD mergers. Experiencing binary evolution, these merger products have older true ages than their photometric isochrone ages. According to the AVR in the Milky Way disk, older stars have higher velocity dispersion. So, the fraction of double-WD merger products (f_m) can be estimated from the velocity distribution of high-mass WDs.

We select a homogeneous sample of high-mass WDs ($0.8\text{--}1.3 M_{\odot}$, $d < 250 \text{ pc}$) from *Gaia* DR2, which includes

1395 objects. Our sample is about thirty times larger than that of a previous study with a similar idea (Wegg & Phinney 2012). We infer f_m in five mass bins using a Bayesian model of WD transverse velocities. We find

1. about 20% of $0.8\text{--}1.3 M_\odot$ WDs originate from double-WD mergers;
2. the corresponding double-WD merger rates in our mass range add up to $1.1 \times 10^{-13} M_\odot^{-1} \text{yr}^{-1}$.

We show f_m and the merger rate as a function of mass in Figures 3 and 4, respectively. We estimate our systematic error to be within 30%, i.e., a factor of 0.7–1.3. Our results are in good agreement with the predictions from binary population synthesis (see Appendix for setting details).

Our estimates add significant precision and mass resolution to our knowledge of the double-WD merger rate. If it is allowed to extrapolate the estimates to a higher mass range, our results suggest that double-WD mergers can contribute to a significantly large fraction of SNe Ia.

In a few years, the increasing astrometric and photometric precision provided by future *Gaia* data releases and the radial velocity measurements of WDs by future surveys such as SDSS-V (e.g., Kollmeier et al. 2017) will enlarge the available sample size of high-mass WDs and allow for even tighter constraints. We are starting to be able to reliably and precisely compare the observed double-WD merger rates with binary population synthesis, which will shed light upon the progenitor problem of SNe Ia.

We thank the referee Dan Maoz for his valuable suggestions. S.C. thanks Siyu Yao for her constant encouragement and inspiration. J.C. would like to acknowledge his support from the National Science Foundation (NSF) through grant AST-1614933. B.M. thanks the David and Lucile Packard Foundation. S.T. acknowledges support from the Netherlands Research Council NWO (grant VENI No. 639.041.645).

This work has made use of data from the European Space Agency (ESA) mission *Gaia* (<https://www.cosmos.esa.int/gaia>), processed by the *Gaia* Data Processing and Analysis Consortium (DPAC, <https://www.cosmos.esa.int/web/gaia/dpac/consortium>). Funding for the DPAC has been provided by national institutions, in particular the institutions participating in the *Gaia* Multilateral Agreement.

Software: astropy package (Astropy Collaboration et al. 2013, 2018), emcee (Foreman-Mackey et al. 2013), numpy (Oliphant 2006), matplotlib (Hunter 2007), SciPy (Virtanen et al. 2020).

Appendix The Binary Population Synthesis

Here we describe the binary population synthesis that we use in this paper to derive the delay-time distribution. The models are synthesized using the binary population synthesis code SeBa (Portegies Zwart & Verbunt 1996; Toonen et al. 2012). The models are identical to the default models used in Toonen et al. (2017). We have adopted a Kroupa initial mass function (Kroupa et al. 1993) and a uniform mass ratio distribution between 0 and 1 (Raghavan et al. 2010; Duchêne & Kraus 2013). Furthermore, we assume a uniform distribution in the logarithmic semimajor axis up to $10^6 R_\odot$ (Abt 1983), and

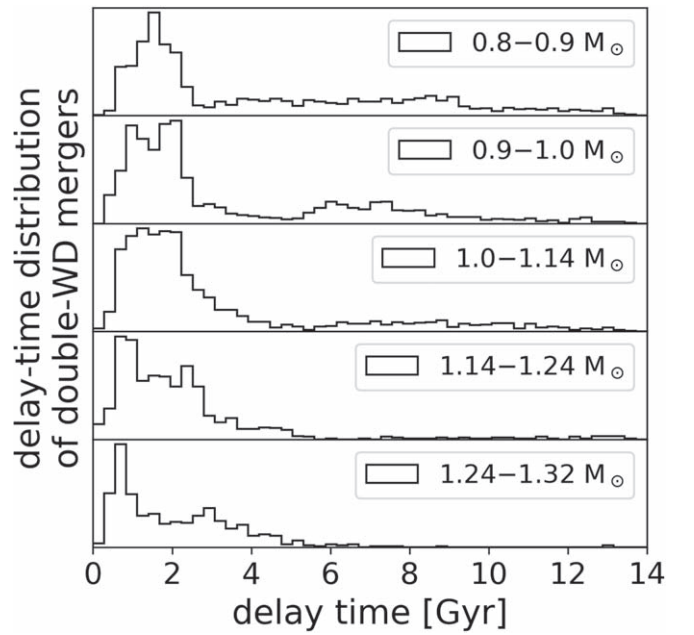


Figure 5. Delay-time distributions of double-WD mergers used in our model. These distributions are generated from binary population synthesis. The x-axis is the delay time of binary evolution, i.e., $\tau - t_{\text{cool}}$ for the resulting WD. The y-axis is in linear scale and normalized to their maximum values. We input to our model the shapes of these five distributions as probability distribution and do not use the information from their normalization.

a thermal distribution of eccentricities between 0 and 1 (Heggie 1975).

One of the main sources of uncertainty in the synthetic populations (Toonen et al. 2014) is a phase of unstable mass transfer, i.e., the common-envelope (CE) phase (for a review, see Ivanova et al. 2013). Similar to Toonen et al. (2017), we apply the “ $\gamma\alpha$ ” model. This model reproduces the mass ratio distribution (Toonen et al. 2012) and number density (Toonen et al. 2017) of double-WD systems best. In the “ $\gamma\alpha$ ” model, we apply the classical (α)-CE that is based on energy conservation (Webbink 1984), and the (γ)-modeling that is based on a balance of angular momentum (Nelemans et al. 2000). Regarding the former the parameters $\alpha\lambda = 2$ describe how efficient orbital energy can be used to unbind the envelope and how strong the envelope is bound to the donor star, and regarding the latter the parameter $\gamma = 1.75$ describes the efficiency of angular momentum usage. The γ -modeling is applied unless the binary contains a compact object or the CE is triggered by a tidal instability. We note that for our purpose to compare the merger rate, the delay-time distribution of the “ $\gamma\alpha$ ” model does not significantly differ from that of the model that exclusively adopts the α -CE with $\alpha\lambda = 2$ (see Toonen et al. 2012).

Figure 5 shows the delay-time distributions in five mass bins, which are used in our kinematic analysis. For the synthesized merger rates shown in Figure 4, we in addition assume a 50% binary fraction of all stars (see also Duchêne & Kraus 2013; Moe & Di Stefano 2017).

ORCID iDs

Sihao Cheng (程思浩) <https://orcid.org/0000-0002-9156-7461>
 Jeffrey D. Cummings <https://orcid.org/0000-0001-7453-9947>
 Silvia Toonen <https://orcid.org/0000-0002-2998-7940>

References

- Abt, H. A. 1983, *ARA&A*, 21, 343
- Arenou, F., Luri, X., Babusiaux, C., et al. 2018, *A&A*, 616, A17
- Astropy Collaboration, Price-Whelan, A. M., Sipőcz, B. M., et al. 2018, *AJ*, 156, 123
- Astropy Collaboration, Robitaille, T. P., Tollerud, E. J., et al. 2013, *A&A*, 558, A33
- Badenes, C., & Maoz, D. 2012, *ApJL*, 749, L11
- Bhattacharya, M., Mukhopadhyay, B., & Mukerjee, S. 2018, *MNRAS*, 477, 2705
- Binney, J., & Tremaine, S. 2008, *Galactic Dynamics* (2nd ed.; Princeton, NJ: Princeton Univ. Press)
- Bovy, J. 2017, *MNRAS*, 468, L63
- Brown, W. R., Gianninas, A., Kilic, M., Kenyon, S. J., & Allende Prieto, C. 2016a, *ApJ*, 818, 155
- Brown, W. R., Kilic, M., Kenyon, S. J., & Gianninas, A. 2016b, *ApJ*, 824, 46
- Brown, W. R., Kilic, M., Kosakowski, A., et al. 2020, *ApJ*, 889, 49
- Camisassa, M. E., Althaus, L. G., Córscico, A. H., et al. 2019, *A&A*, 625, A87
- Cheng, S., Cummings, J. D., & Ménard, B. 2019, *ApJ*, 886, 100
- Choi, J., Dotter, A., Conroy, C., et al. 2016, *ApJ*, 823, 102
- Cummings, J. D., Kalirai, J. S., Tremblay, P.-E., Ramirez-Ruiz, E., & Choi, J. 2018, *ApJ*, 866, 21
- Dan, M., Rossow, S., Brüggen, M., & Podsiadlowski, P. 2014, *MNRAS*, 438, 14
- Duchêne, G., & Kraus, A. 2013, *ARA&A*, 51, 269
- Dunlap, B. H., & Clemens, J. C. 2015, in *ASP Conf. Ser.* 493, 19th European Workshop on White Dwarfs, ed. P. Dufour, P. Bergeron, & G. Fontaine (San Francisco, CA: ASP), 547
- El-Badry, K., & Rix, H.-W. 2018, *MNRAS*, 480, 4884
- Evans, D. W., Riello, M., De Angeli, F., et al. 2018, *A&A*, 616, A4
- Fontaine, G., Brassard, P., & Bergeron, P. 2001, *PASP*, 113, 409
- Foreman-Mackey, D., Hogg, D. W., Lang, D., & Goodman, J. 2013, *PASP*, 125, 306
- Gaia Collaboration, Babusiaux, C., van Leeuwen, F., et al. 2018a, *A&A*, 616, A10
- Gaia Collaboration, Brown, A. G. A., Vallenari, A., et al. 2018b, *A&A*, 616, A1
- Gaia Collaboration, Prusti, T., de Bruijne, J. H. J., et al. 2016, *A&A*, 595, A1
- Gentile Fusillo, N. P., Tremblay, P.-E., Gänsicke, B. T., et al. 2019, *MNRAS*, 482, 4570
- Giammichele, N., Bergeron, P., & Dufour, P. 2012, *ApJS*, 199, 29
- Han, Z. 1998, *MNRAS*, 296, 1019
- Heggie, D. C. 1975, *MNRAS*, 173, 729
- Holberg, J. B., & Bergeron, P. 2006, *AJ*, 132, 1221
- Hunter, J. D. 2007, *CSE*, 9, 90
- Iben, I., Jr., & Tutukov, A. V. 1984, *ApJS*, 54, 335
- Iben, I., Jr., Tutukov, A. V., & Yungelson, L. R. 1996, *ApJ*, 456, 750
- Ivanova, N., Justham, S., Chen, X., et al. 2013, *A&AR*, 21, 59
- Just, A., & Jahreiß, H. 2010, *MNRAS*, 402, 461
- Kollmeier, J. A., Zasowski, G., Rix, H.-W., et al. 2017, arXiv:1711.03234
- Kowalski, P. M., & Saumon, D. 2006, *ApJL*, 651, L137
- Kroupa, P., Tout, C. A., & Gilmore, G. 1993, *MNRAS*, 262, 545
- Li, W., Chornock, R., Leaman, J., et al. 2011, *MNRAS*, 412, 1473
- Lindgren, L., Hernández, J., Bombrun, A., et al. 2018, *A&A*, 616, A2
- Liu, D., Wang, B., Wu, C., & Han, Z. 2017, *A&A*, 606, A136
- Lorén-Aguilar, P., Isern, J., & García-Berro, E. 2009, *A&A*, 500, 1193
- Maoz, D., Badenes, C., & Bickerton, S. J. 2012, *ApJ*, 751, 143
- Maoz, D., & Graur, O. 2017, *ApJ*, 848, 25
- Maoz, D., & Hallakoun, N. 2017, *MNRAS*, 467, 1414
- Maoz, D., Hallakoun, N., & Badenes, C. 2018, *MNRAS*, 476, 2584
- Maoz, D., Mannucci, F., & Nelemans, G. 2014, *ARA&A*, 52, 107
- Maoz, D., Sharon, K., & Gal-Yam, A. 2010, *ApJ*, 722, 1879
- Marsh, T. R. 1995, *MNRAS*, 275, L1
- Marsh, T. R., Dhillon, V. S., & Duck, S. R. 1995, *MNRAS*, 275, 828
- McMillan, P. J. 2011, *MNRAS*, 414, 2446
- Mennekens, N., Vanbeveren, D., De Greve, J. P., & De Donder, E. 2010, *A&A*, 515, A89
- Moe, M., & Di Stefano, R. 2017, *ApJS*, 230, 15
- Nelemans, G., Verbunt, F., Yungelson, L. R., & Portegies Zwart, S. F. 2000, *A&A*, 360, 1011
- Nordström, B., Mayor, M., Andersen, J., et al. 2004, *A&A*, 418, 989
- Oliphant, T. E. 2006, *A Guide to NumPy*, Vol. 1 (USA: Trelgol Publishing)
- Perets, H. B., Zenati, Y., Toonen, S., & Bobrick, A. 2019, arXiv:1910.07532
- Portegies Zwart, S. F., & Verbunt, F. 1996, *A&A*, 309, 179
- Raghavan, D., McAlister, H. A., Henry, T. J., et al. 2010, *ApJS*, 190, 1
- Rebassa-Mansergas, A., Rybicka, M., Liu, X.-W., Han, Z., & García-Berro, E. 2015, *MNRAS*, 452, 1637
- Riello, M., De Angeli, F., Evans, D. W., et al. 2018, *A&A*, 616, A3
- Ruiter, A. J., Belczynski, K., & Fryer, C. 2009, *ApJ*, 699, 2026
- Sato, Y., Nakasato, N., Tanikawa, A., et al. 2015, *ApJ*, 807, 105
- Schwab, J. 2019, *ApJ*, 885, 27
- Shen, K. J., Boubert, D., Gänsicke, B. T., et al. 2018a, *ApJ*, 865, 15
- Shen, K. J., Kasen, D., Miles, B. J., & Townsley, D. M. 2018b, *ApJ*, 854, 52
- Shen, K. J., Toonen, S., & Graur, O. 2017, *ApJL*, 851, L50
- Sollima, A. 2019, *MNRAS*, 489, 2377
- Temmink, K. D., Toonen, S., Zapartas, E., Justham, S., & Gänsicke, B. T. 2019, arXiv:1910.05335
- Toonen, S., Claeys, J. S. W., Mennekens, N., & Ruiter, A. J. 2014, *A&A*, 562, A14
- Toonen, S., Hollands, M., Gänsicke, B. T., & Boekholt, T. 2017, *A&A*, 602, A16
- Toonen, S., Nelemans, G., & Portegies Zwart, S. 2012, *A&A*, 546, A70
- Tremblay, P.-E., Bergeron, P., & Gianninas, A. 2011, *ApJ*, 730, 128
- Tremblay, P.-E., Cummings, J., Kalirai, J. S., et al. 2016, *MNRAS*, 461, 2100
- Tutukov, A. V., Yungelson, L. R., & Iben, I., Jr. 1992, *ApJ*, 386, 197
- Virtanen, P., Gommers, R., Oliphant, T. E., et al. 2020, *Nat. Methods*, 17, 261
- Webbink, R. F. 1984, *ApJ*, 277, 355
- Wegg, C., & Phinney, E. S. 2012, *MNRAS*, 426, 427
- Yungelson, L. R., & Kuranov, A. G. 2017, *MNRAS*, 464, 1607